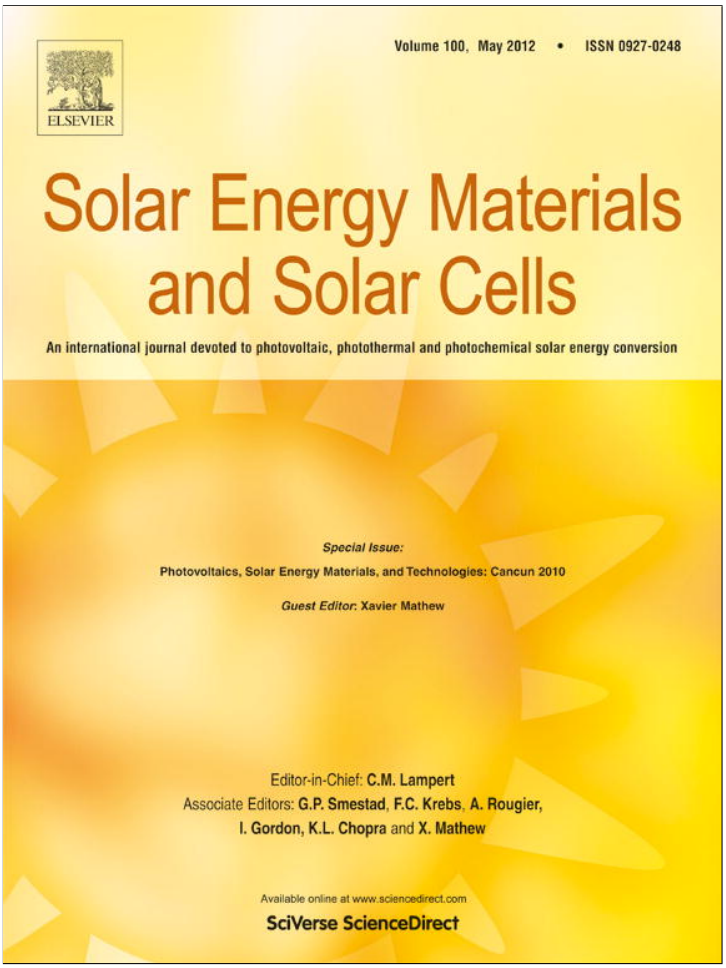

Solar Energy Materials & Solar Cells 100 (2012) 185–191

Contents lists available at SciVerse ScienceDirect

Solar Energy Materials & Solar Cells

journal homepage: www.elsevier.com/locate/solmat

Oxygen doping-induced photogeneration loss in P3HT:PCBM solar cells

Antonio Guerrero [a,*], Pablo P. Boix [a], Luís F. Marchesi [a,b], Teresa Ripolles-Sanchis [a], Ernesto C. Pereira [b], Germà Garcia-Belmonte [a,*]

[a] Photovoltaic and Optoelectronic Devices Group, Departament de Física, Universitat Jaume I, ES-12071 Castelló, Spain
[b] Laboratório Interdisciplinar de Electroquímica e Cerâmica (LIEC), Universidade Federal de São Carlos, São Carlos, Brazil

ARTICLE INFO

Article history:
Received 5 December 2011
Received in revised form
5 January 2012
Accepted 14 January 2012
Available online 7 February 2012

Keywords:
Organic photovoltaics
Oxygen doping
Capacitance
Degradation

ABSTRACT

This work investigates the loss in performance induced by molecular oxygen in bulk heterojunction solar cells. We observe that upon exposure to molecular oxygen both formation of $P3HT^+:O_2^-$ complex and metal oxidation at the interface between the active layer and metallic contact occur. These two different effects were separately investigated using $NOBF_4$ as an oxidant. Our procedure has allowed studying p-doping of the active layer independently from contact degradation. A loss in photocurrent is associated with formation of $P3HT^+:O_2^-$ complex, which reduces the concentration of neutral P3HT present in the film in accordance with absorption and external quantum efficiency spectra. This complex is regarded as a source of a pathway of reversible degradation. Capacitance–voltage measurements allow for an accurate extraction of p-doping levels of the active layer produced by the presence of charged O_2^- species. In addition, one of the irreversible degradation pathways is identified to be oxidation of the metallic contact to form CaO. This oxide forms a thin dipole layer producing a voltage drop across the active layer/Ca interface, which has a direct impact on the open circuit voltage and fill factor.

1. Introduction

Organic solar cells have attracted much attention over the last decade, and currently power conversion efficiencies over 8% have been reported [1]. In order to obtain further improvements in long-term solar cell performance a detailed understanding of the device stability and degradation mechanisms is required [2]. Known degradation mechanisms include diffusion of molecular oxygen and water into the device [3], degradation of interfaces [4], degradation of the active material [5], interlayer and electrode diffusion[6] or electrode reaction with the organic materials [7]. In regular architecture solar cells prepared in ambient conditions oxygen has always been regarded as a source of cell performance losses [8]. In terms of chemical modifications oxygen plays an important role as it is responsible for chemical degradation pathways in the dark and, more rapidly, in combination with light [4]. Indeed, degradation of systems comprising P3HT [9] and C_{60} [10,11] induced by oxygen has been reported to decrease carrier mobilities and enhance trap densities. Additionally, the effect of oxygen has normally been related to degradation of the metallic aluminium or calcium contact to form oxides in a regular configuration [12].

There is some controversy on the role of oxygen as a degradation source. On one hand, P3HT has been reported to form a complex with oxygen [13,14]. However, in the solid state even at high concentrations of singlet oxygen the solid film has been reported to remain unaltered [15]. Thus, degradation of the film appears to take place through a radical mechanism that requires overcoming an activation energy [16]. Interestingly, recent studies on degradation pathways induced by oxygen of semi-permeable bulk heterojunction cells have identified components of both reversible and irreversible degradations [17]. In that work, reversible degradation of the cells in the presence of oxygen resulted mainly in the reduction of short circuit current, while the loss in light absorption was negligible. However, we experimentally observe by submitting the cells to a controlled oxygen exposure that a simultaneous decrease in both photocurrent and absorption exists in agreement with the increase of p-doping level extracted from capacitance–voltage analysis. A direct connection is then established between an oxygen-related degradation route and cell performance parameters.

The specific goal of our work is to understand the effects of oxygen on the active layer blend (P3HT:PCBM) and contact in bulk heterojunction cells of regular configuration. Since the metallic contact oxidation may occur simultaneously with the blend degradation, we follow a robust fabrication method in air

* Corresponding authors. Tel.: +34 964 387463; fax: +34 964 729218.
E-mail addresses: aguerrer@uji.es (A. Guerrero), garciag@uji.es (G. Garcia-Belmonte).

0927-0248/$ - see front matter © 2012 Elsevier B.V. All rights reserved.
doi:10.1016/j.solmat.2012.01.012

and treat the samples with different oxidant sources prior to cathode deposition. The cell preparation procedure allows us to separate degradation contributions originated at the device bulk from those occurring at the outer interface. Recently, regular organic solar cells fabricated in air have been reported to provide similar performances to those of devices produced under a nitrogen atmosphere [18]. This fact would suggest that the origin of device degradation is not induced during device fabrication, but because of oxygen or water diffusion. Hence chemical degradation begins to be evident only after the cathode has been deposited and the cell has been completed. The present work demonstrates the formation of a P3HT complex with oxygen (highly reversible), which is related to the photocurrent decrease and monitored through capacitance–voltage measurements. Additionally, generation of metallic oxide layers as CaO at the cathode contact interface (completely irreversible) is observed.

2. Experimental

2.1. Samples preparation and oxygen exposure

In this work we follow photovoltaic cells fabrication process carried out in air [18]. A detailed description of the experimental conditions can be found in Appendix A. We briefly describe here the process for our control cell (cell 1, Table 1). First, we prepared all the mixed P3HT:PCBM solutions in a glovebox filled with a nitrogen atmosphere using dry *o*-dichlorobenzene (ODCB). Films are spin cast in air and the active layer was "solvent annealed" in a Petri dish for 2 h. At this point cells were transferred to the glovebox to undergo a thermal annealing treatment to provide an "oxygen free" active layer. For our photovoltaic cells we found optimum cell efficiencies when heated at 150 °C for 10 min and these conditions were used for all devices described in this work. Cell 1 was kept in the glovebox throughout the time from the thermal treatment to device encapsulation [19]. Note that device encapsulated is required to avoid oxygen contamination from the environment. The polymer solar cells were fabricated with a standard sandwich structure of ITO/PEDOT:PSS/P3HT:PCBM/Ca/Ag.

As reported by Mattis et al. [20] the annealing temperature required to promote oxygen desorption needs to be above 120 °C. Thus, we did not carry out a second thermal treatment after contact evaporation, which usually improves cell performance. For oxygen doped samples a second annealing treatment would induce oxygen desorption and in that case we would not be able to measure the intentionally introduced oxygen doping (see Table 1). Hence only one annealing step is necessary to obtain an adequate morphology and to provide effective oxygen desorption in P3HT prior to cathode deposition. As a result optimum efficiencies were found for devices with an active layer thickness of 400 nm. This is considerably higher than values usually reported in P3HT:PCBM photovoltaic cells (ca. 150–250 nm). All the cells presented in this study followed this processing; introduction of oxygen or a different oxidant into the system was carried out as explained below.

Oxygen treatment is implemented at different stages. For sample 2, traces of water that may be present in the films (i.e. PEDOT:PSS is highly hygroscopic) are carefully eliminated in the glovebox after the "solvent cure" step. The substrate was placed under vacuum and was heated to 50 °C for 1 h. Further traces of water were eliminated by introducing the sample in a high vacuum chamber in the glovebox at a pressure of 1×10^{-6} mbar overnight. After this exhaustive elimination of water the film was annealed to obtain an adequate morphology. The sample was placed in a sealed portable chamber with no-return valves to provide a flow of dry synthetic compressed air (ca. nitrogen 80% and oxygen 20%) for 2 h. Cells 3 and 4 were treated with dry synthetic compressed air after annealing in the same setup without exhaustively removing traces of water. Finally, sample 5 was doped with molecular oxygen by saturation of the P3HT:PCBM solution with dry oxygen before spin coating.

In a second set of experiments $NOBF_4$ was used as the oxidant. For cells 6–8 this oxidant is introduced in the system before spincasting the active layer. P3HT reacts with $NOBF_4$ to provide a very dark solution and a solid. The reaction product was added to the P3HT:PCBM blend to provide the $NOBF_4$ concentration described in Table 1 ($\sim1\times10^{-6}$ M). On the other hand, sample 9 was treated with $NOBF_4$ in acetonitrile directly after spin-coating the active layer at considerably higher concentration (1×10^{-2} M).

3. Results

3.1. Current density–voltage curves

Fig. 1 shows the current density–voltage curves for all analyzed samples and Table 2 summarizes their photovoltaic parameters. Optimum efficiencies were found for devices with an active layer thickness of 400 nm. Considering this large thickness, the reference sample (cell 1) shows a relatively high efficiency (2.8%) with high fill factor (FF) and open circuit voltage (V_{oc}). However, the short circuit current (J_{sc}) is considerably lower than that obtained for thinner cells which are reported to provide 10 mA cm^{-2} [21]. Cells doped with oxygen show decreased performance with increasing oxygen exposure. Cell 2 that was meticulously dried and treated with dry synthetic air for 2 h shows very similar results to those obtained for the reference cell. Cell 3 (1 h oxygen treatment and no additional drying step) shows similar V_{oc} to that of the reference cell and cell 2. However, the J_{sc} was slightly reduced and the FF decreases from 58% for cell 1 to 45% for cell 3. An additional hour of exposure to oxygen of cell 4 further decreased the photocurrent and the photovoltage began to be affected. Modifying the exposure method to oxygen for cell 5 provided very similar device parameters to those of cell 4 with slightly reduced V_{oc} and increased FF.

Table 1
Summary of preparation method and main characteristics.

ID	Dopant	Method	Time/concentration	Notes
1	None	–	–	Reference cell
2	O_2	Flow of dry air passed through film in a chamber in the dark	2 h	Exhaustive drying step
3	O_2	Flow of dry air passed through film in a chamber in the dark	1 h	
4	O_2	Flow of dry air passed through film in a chamber in the dark	2 h	
5	O_2	Dry air bubbled through active layer solution in the dark	10 min	
6	$NOBF_4$	Dopant added to active layer solution	5×10^{-7} M	Stock solution in dichlorobenzene
7	$NOBF_4$	Dopant added to active layer solution	1×10^{-6} M	Stock solution in dichlorobenzene
8	$NOBF_4$	Dopant added to active layer solution	2×10^{-6} M	Stock solution in dichlorobenzene
9	$NOBF_4$	Dopant added to active layer solution	1×10^{-2} M	Stock solution in acetonitrile, and LiF/Al cathode contact

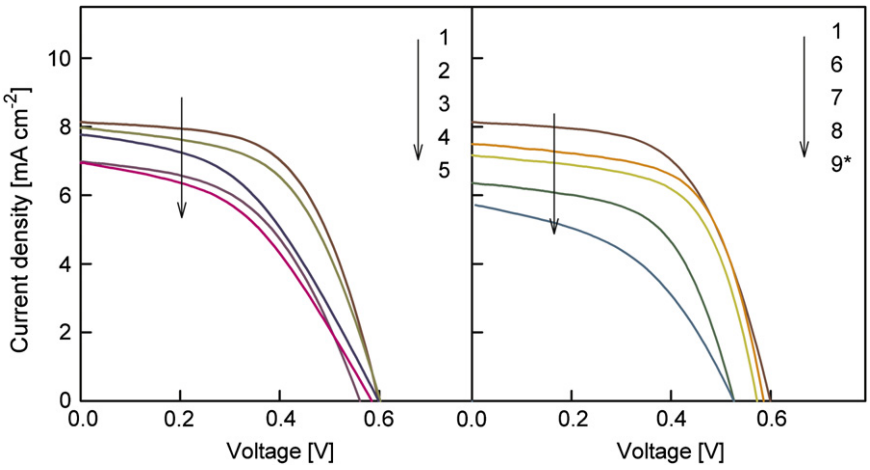

Fig. 1. Representation of the current density–voltage curves of photovoltaic cells doped under different oxidant conditions: molecular oxygen (left) and $NOBF_4$ (right). *A different metallic contact was used (LiF/Al/Ag).

Table 2
Performance summary of solar cells with doping levels and V_{fb} extracted from *C–V* measurements.

ID	J_{sc} (mA cm^{-2})	V_{oc} (mV)	FF (%)	PCE (%)	n ($\times 10^{16}$ cm^{-3})	V_{fb} (mV)
1	8.13	598	58	2.8	0.9	467
2	7.98	601	55	2.6	1.1	543
3	7.77	600	45	2.1	1.1	455
4	6.94	580	45	1.8	1.5	438
5	6.99	560	50	1.9	2.3	419
6	7.50	585	62	2.7	1.8	456
7	7.17	572	61	2.5	3.5	471
8	6.36	525	57	1.9	4.4	507
9	5.74	525	45	1.4	10.8	390

A second set of devices used $NOBF_4$ as the oxidizing agent. We followed a fabrication process analogous to that employed for cell 5 but using $NOBF_4$ in solution instead of dry synthetic air. The current density–voltage curves for cells doped with $NOBF_4$ are shown in Fig. 1 (right). As occurrs for oxygen doping, an increment in solution concentration containing $NOBF_4$ decreases J_{sc} and V_{oc} gradually. However, in contrast to samples doped with oxygen, where the FF is reduced significantly, devices doped with $NOBF_4$ show only a slight decrease for sample 8. Processing conditions for sample 9 involved high concentrations of $NOBF_4$. It should be noticed that in order to obtain a working device with conditions for cell 9, a different metallic contact was used (LiF/Al/Ag). Interestingly, the replacement of the metallic contact for both helps to recover device performance (from 0.006% to 1.4%). A detailed discussion can be found in Appendix A.

3.2. Optical properties of materials, and films and relation with EQE

In order to understand whether the reaction of P3HT:PCBM blend with molecular oxygen gives rise to similar polymer oxidation as those obtained with $NOBF_4$ we carried out characterization by absorption measurements in solution. First a solution containing PCBM in ODCB was treated with either molecular oxygen or $NOBF_4$ at room temperature and no spectroscopic difference was observed after 24 h. Then, a solution containing P3HT in ODCB was treated with dry oxygen for 30 s at room temperature. The spectrum is shown in Fig. 2 and clearly shows that the creation of new species reduces the intensity of the absorption peak of P3HT as this polymer takes part in complex formation. A new absorption band is generated towards the

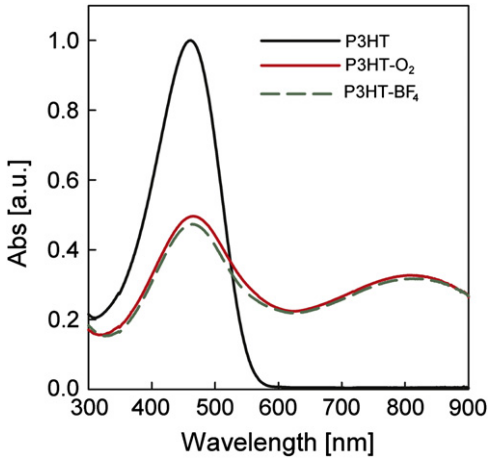

Fig. 2. Comparison of UV–vis spectra of P3HT in *o*-dichlorobenzene solution with the spectra of the P3HT solution after exposure to molecular oxygen ($P3HT^+–O_2^-$) and $NOBF_4$ ($P3HT–BF_4^-$).

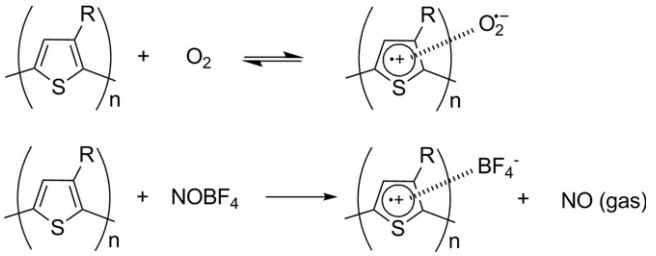

Scheme 1. Transfer complex formation of P3HT in the presence of oxygen as proposed in literature (top) and proposed reaction of P3HT with the oxidant $NOBF_4$ (bottom).

infrared with a maximum peak at 810 nm, which is attributed to polaronic transitions [22]. This new band is then assigned here to the complex $P3HT^+:O_2^-$ formed by reaction of P3HT and oxygen (Scheme 1, top) [13]. Additionally, the reaction product between P3HT and $NOBF_4$ was also characterized by absorption measurements. Both reactions of P3HT with either O_2 or $NOBF_4$ produce similar absorption response in solution using ODCB as solvent. Chemically the main difference between both oxidants is that in this last case we expect the reaction to be irreversible as

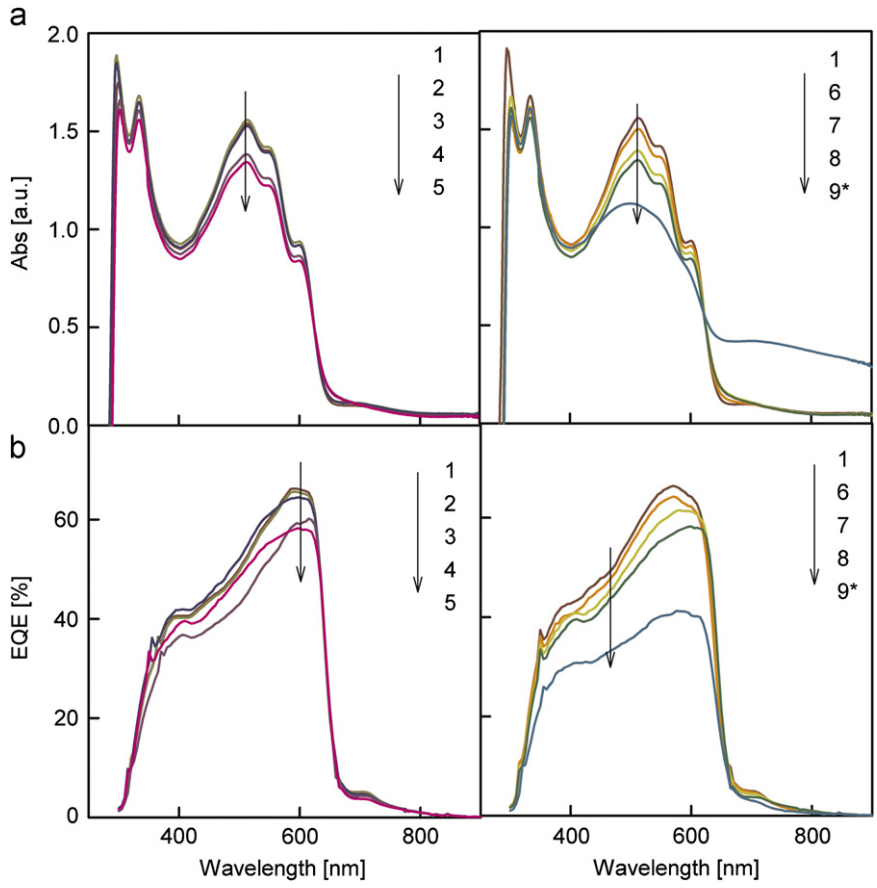

Fig. 3. Correlation between film absorption spectra (a) and EQE spectra of completed cells (b) for different oxidant conditions: molecular oxygen (left) and $NOBF_4$ (right). *A different metallic contact was used (LiF/Al/Ag).

NO gas is evolved (Scheme 1, bottom) the counterion being BF_4^- for the second oxidant.

In order to analyze the effect of oxygen doping on the photocurrent we measure the steady-state absorption of films processed under the same conditions of the referred cells (without the cathode contact). Films 1–3 exhibit similar absorption spectra in terms of intensities and absorption onsets (Fig. 3a, left). These findings are in perfect agreement with those discussed by Seeman et al. [17], in which they did not observe any change in the absorption intensity with exposure to dry synthetic air. However, films 4 and 5 show reduced absorption intensity for P3HT and, interestingly, the intensity in absorption in the 650–700 nm region is slightly altered. Similarly, films doped with $NOBF_4$ confirmed the same trend observed for oxygen doping. Increasing the concentration of $NOBF_4$ led to decreased intensity of the P3HT absorption and increased absorption towards long wavelengths.

EQE measurements of the corresponding cells were also performed. A correlation for all cells under study between intensities obtained from absorption spectra and EQE is clear: reduced absorption led to reduced charge collection in the same proportion. Interestingly, none of the cells show increase of charge collection in the 700–800 nm region. This is especially noticeable for cell 9 using high $NOBF_4$ concentration, which despite showing a clear band in the red region does not contribute to the extracted charges as inferred from EQE measurements.

3.3. Capacitance–voltage analysis.

Analysis of capacitance–voltage (C–V) measurements has become a standard technique to extract relevant material parameters. In previous work, we showed that for organic photovoltaics information extracted from C–V measurements are related to the p-doping level resulting from defect states within the polymer band gap [23]. Standard P3HT:PCBM solar cells showed Mott–Schottky characteristics, exhibiting full depletion at reverse bias and a linear relationship at low forward bias (0.0–0.5 V) [23]. The density of fully ionized defect states (p-doping level) n was derived from the slope by means of the Mott–Schottky relation

$$C^{-2} = \frac{2(V_{fb} - V)}{A^2 q \varepsilon \varepsilon_0 n} \quad (1)$$

where A corresponds to the device active surface, ε is the relative dielectric constant of the blend, ε_0 the permittivity of the vacuum and n the total concentration of acceptor impurities (intrinsic

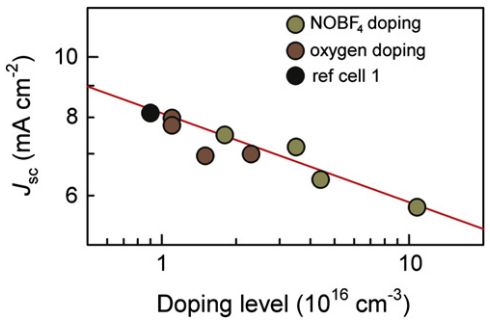

Fig. 4. Correlation between short-circuit current density and doping level. Data correspond to reference cell 1, and oxygen and $NOBF_4$ treated cells. The experimental relationship $J_{sc} \propto n^{-0.14}$ is encountered.

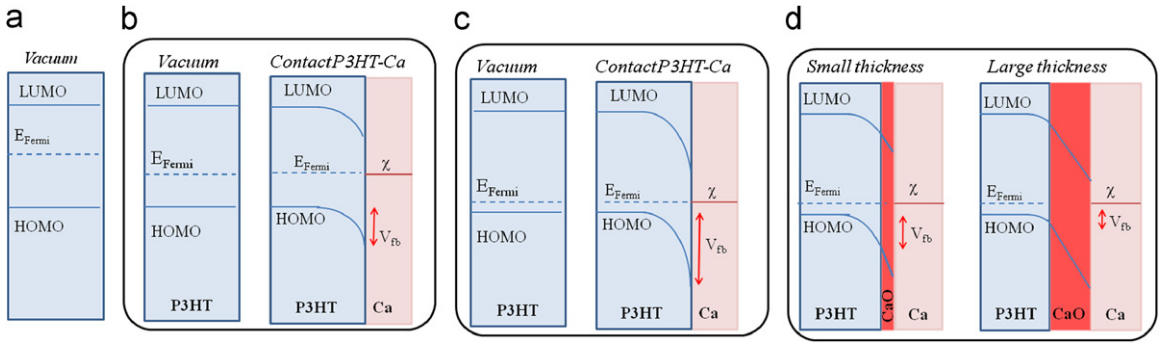

Fig. 5. Energy diagrams of an organic semiconductor showing the effect of a variation of doping levels and presence of a dielectric interlayer (CaO): (a) un-doped semiconductor, (b) semiconductor p-type doped, (c) semiconductor heavily p-doped and (d) effect of CaO thickness.

defects with additional charged immobile O_2^- or BF_4^- counter-ions). It is assumed that the defect density explored from capacitance corresponds to those defects able to follow measuring frequency. Thus, by analyzing the curve $C^{-2}(V)$ one can extract V_{fb} from the intercept and the total concentration of acceptor impurities from the slope (n). The intercept of this straight line with the real axis is related to the flat-band potential, which corresponds to the energy offset between the hole Fermi level and the cathode metal effective work function (see Fig. 5b). Recently, this technique has been used to monitor oxygen doping levels in polymer solar cells [17].

By analysis of the C–V measurements we were able then to obtain accurate values for p-doping of the polymer. It is worth noting that C–V Mott–Schottky analysis is sensitive only to the density of ionized impurity levels. A Mott–Schottky plot for our devices clearly shows different slopes for the samples exposed to oxygen under different experimental conditions (Appendix A). For clarification, it is important to note that the reported Mott–Schottky plots do not show full depletion at -1 V of reverse bias. An estimation of the geometric capacitance gives rise to a value of 7 nF/cm^2. Taking into account that the capacitance values observed are higher than this and that depletion width is below 100 nm at -1 V we can conclude that full depletion has not been obtained for devices with high doping levels. On the other hand, device 1 shows a depletion width at -1 V of 350 nm, which is close to the device thickness, indicating that at this voltage the cell begins to be fully depleted, and explains why the $C^{-2}(V)$ curve exhibits saturation as cells are reversely polarized (see Appendix A).

The results extracted from Mott–Schottky plots are summarized in Table 1. The total concentration of acceptor impurities (n) confirms the lowest doping level (0.9×10^{16} cm^{-3}) for control sample 1. This minimum doping level corresponds to structural defects of the polymer, and to extrinsic impurities that are inherent to the processing and purity degree of chemicals used. Values for cells treated with oxygen range from 1.0 to 1.5×10^{16} molecules cm^{-3}. Slightly higher values are obtained for cell 5 doped by oxygen saturation of the spin coating solution.

Alternatively, the doping densities of samples doped with a stock solution of $P3HT^+$:BF_4^- (cells 6–8) are clearly higher than those obtained with oxygen. This supports that with $NOBF_4$ used as oxidant irreversible processes take place (oxidant desorption is not possible). Finally, cell 9 doped with a highly concentrated solution of $NOBF_4$ gives rise to the highest doping levels (10.8×10^{16} cm^{-3}).

In addition to the doping levels, V_{fb} was calculated by analysis of the Mott–Schottky characteristics. A baseline flat-band voltage value of 467 mV was obtained for sample 1. This increased for cell 2, treated with oxygen, and followed with a gradual decrease for the subsequent samples. On the other hand, for samples treated with $NOBF_4$, where no oxidation of the metallic contact is expected (cells 4–8) increasing doping concentrations of the oxidant increases V_{fb} from values of 456 to 507 mV. Sample 9 provides a low value of 390 mV. The observed trends will be explained in detail in Section 4.

4. Discussion

4.1. Correlation between photocurrent and doping level.

Our experimental methodology enabled us to treat the P3HT:PCBM layer with oxygen before contacting the cathode metal. As supported by absorption measurements in solution it appears that PCBM does not react with oxidants such as molecular oxygen or $NOBF_4$ in ODCB at room temperature. P3HT does react with molecular oxygen to form $P3HT^+$:O_2^- complexes. We consider such complex formation as a primary source of solar cell long-term degradation. A correlation is observed between the measured doping levels, absorption spectra of the films, EQE results and the photocurrent obtained for operating cells. Thus, cells 1–3 show similar film absorption and EQE spectra with a measured maximum current of $\sim$8 mA/cm^2. On the contrary, cells 4 and 5 exhibit reduced collection of charge carriers to provide a maximum current of $\sim$7 mA/cm^2. These results correlate with the obtained J_{sc}, and corroborate the relationship between oxygen doping and loss in photocurrent through reduction in absorption caused by lower concentration of neutral P3HT. The drop in V_{oc} is explained by a reduction in light absorbed, because fewer photogenerated carriers reduce the occupancy of polymer and fullerene electronic states and then inhibit the Fermi level splitting, which is the ultimate origin of the photovoltage [24]. This type of performance loss is expected to be partially reversible through oxygen desorption via further annealing treatments.

For cells treated with molecular oxygen we observe that under most conditions the density of fully ionized acceptor impurities is increased with respect to those obtained for reference cell 1. Attempts to increase the doping levels from oxygen-free sample 1 to slightly doped sample 2 show this slight effect (Table 1). It is interesting to note that cells 2 and 4 both were exposed to oxygen for 2 h, but the former meticulously dried. Whilst the totally dried cell exhibits similar doping levels to that of reference cell 1, cell 4 shows slightly higher doping levels. By comparison of the performance characteristics of cells 3 and 4 it is clear that the reduced performance is due to additional exposure to oxygen and not to reaction with traces of water. Higher doping concentrations were obtained using a molecular oxygen doping process in solution (cell 5) prior to the annealing step.

Oxidation of the metallic contact with oxygen or water present at the interface was nevertheless expected. Thus, in order to totally avoid generation of CaO and truly understand the effect of oxidants in the active layer we carried out further experiments

with $NOBF_4$. Such an oxidant agent allows us to investigate active layer p-doping without the effect of calcium oxidation. As previously commented upon, P3HT does indeed react with both oxidants, generating analogous reaction products. The main consequence of this is that the P3HT absorption band intensity decreases. This intensity reduction is also observed when film absorption measurements are carried out on the $NOBF_4$ treated samples (Fig. 3a, right). Additionally, a slight increase in the intensity in the 650–700 nm region is also observed for samples 7 and 8 doped with $NOBF_4$. This increase in intensity is assigned to generation of the complex $P3HT^+:BF_4^-$ as supported by the spectra of cell 9 ,whereby the concentration of $NOBF_4$ was increased by 10^4 factor during film preparation. Interestingly, the EQE and current density results obtained for completed doped cells clearly correlate with the film absorption measurements. Note that the newly generated species do not contribute to the collected charges.

The previous findings strongly indicate that the decrease in photocurrent density observed in the complete cells is primary caused by a decrease in light absorption, and not by losses produced during carrier transport to the collecting electrodes. Because collection efficiency diminishes as oxidation level is raised, the observed simultaneous reduction in intensity of both absorption and EQE spectra should be related to a loss in photogeneration of mobile carriers. Additionally, the decrease in photovoltage can also be explained by a decrease in photogeneration as V_{oc} depends on the amount of light absorbed that is able to yield separated charge carriers.

As aforementioned *C–V* analysis provides direct information about the density of dopants that are actually ionized, contributing to the conductivity (p-doping). Therefore oxidant doping modifies the concentration of mobile hole carriers as new chemical species are created. The immobile O_2^- or BF_4^- counterions contribute to the formation of a hole depletion zone near the cathode contact (band bending), which was monitored by the *C–V* technique. As observed, total concentrations of acceptor impurities are qualitatively in agreement with the spectroscopic measurements and the decrease in photocurrent observed for the complete cells. Fig. 4 illustrates this correlation, including all cells studied. As observed an experimental relationship $J_{sc} \propto n^{-0.14}$ is found between photocurrent and doping level extracted from *C–V* analysis. However it is hard to understand how an increment of p-doping level within one order of magnitude (from $\sim 10^{16}\,cm^{-3}$ up to $10^{17}\,cm^{-3}$) is able to induce such a large decrease in light absorption, which gives rise to ~33% reduction in photocurrent (from $8.13\,mA\,cm^{-2}$ down to $5.74\,mA\,cm^{-2}$). Oxidation levels as calculated from the *C–V* analysis are only in the range of 0.1–0.01% of polymer monomers taking part in the reactions drawn in Scheme 1. This apparent discrepancy can be solved by recalling that *C–V* analysis only monitors the density of fully ionized charge species (those participating in the modulation of the depletion zone). It is then necessary to distinguish between O_2^- (or BF_4^-) counterion able to yield mobile hole carriers, from those that keep the hole attached forming the neutral complex $P3HT^+:O_2^-$ (or $P3HT^+:BF_4^-$). Therefore we remark that only a portion of the total oxidized polymer units contribute to increase the mobile hole concentration.

4.2. Effect of metal cathode oxidation

Regarding the variation in V_{fb} observed for cells doped with oxygen, Fig. 5 shows different energy diagrams that explain the effect of increasing the p-doping concentration. An undoped semiconductor before contacting exhibits an energy diagram as that showed in Fig. 5a. The difference in energy between the Fermi level (E_F) and the HOMO will be the same as the difference in energy between E_F and the LUMO. As the material is doped (p-type), E_F will shift on approaching the HOMO of the polymer. The difference in energy between the HOMO and E_F will become smaller as we increase the concentration of p-dopants (Fig. 5b and c). In addition, when the active layer is placed in contact with a metal, E_F and the effective work function of the metal equilibrate at the interface. This equilibration gives rise to band bending (electrical field confinement) at the interface vicinity [23]. The flat band potential equals the energy offset between the hole Fermi level and the effective cathode work function. As p-doping is increased the position of the Fermi level will shift towards low energies, producing an increment in V_{fb}. This situation is clearly observed for samples treated with $NOBF_4$, where no oxidation of the metallic contact has taken place. Thus, V_{fb} increases with increasing doping concentrations as the hole E_F approaches further the HOMO of the P3HT.

Evidences for CaO generation are found for samples treated with oxygen. For cells 2–5, V_{fb} gradually decreases from values of 543 mV (sample 2) to 419 mV (sample 5). By comparison of cells 5 and 6 with similar doping levels, it is clear from the values obtained from V_{fb} that oxidation of calcium takes place faster for the sample containing molecular oxygen as dopant. This indicates that upon exposure to oxygen, part of the molecular oxygen will produce $P3HT^+:O_2^-$ complexes, while other part will generate calcium oxide. Generation of CaO will then be responsible for a drop in V_{fb} as schematically depicted in Fig. 5c and d [25]. This oxide accommodates part of the applied voltage during *C–V* measurement because of the formation of a dipole layer. Similar energy level shifts have been reported previously for organic/metal interfaces [26]. Thus, an increase in the oxygen exposure provides simultaneously P3HT p-doping increment and decrease in V_{fb}. It is important to note that generation of CaO has taken place to a very small degree as supported by a slightly increased series resistance observed for the sample doped with molecular oxygen (see Appendix A). Presence of CaO clearly has a negative impact on FF, which reduces from nearly 60 to 45, contrary to the case of using $NOBF_4$ as dopant. It is interesting to note that cells doped with $NOBF_4$ (samples 6–8) benefit from high FF regardless of the doping concentration. This indicates that the presence of the complex $P3HT^+:BF_4^-$ does not have a negative impact on the FF. On the other hand, FF was significantly reduced when contact oxidation had taken place.

5. Conclusions

In conclusion this work shows the origin of performance parameter degradation produced by oxygen treatment of the active layer. The different effects induced by oxygen were separated using $NOBF_4$ as an oxidant. Evidences for generation of the complex $P3HT^+:O_2^-$ have been shown on complete cells. This complex is responsible for photocurrent reduction. Loss in photovoltage for cells doped with molecular oxygen is in agreement with the reduced light absorption that generates less charge carriers, inhibiting the Fermi level splitting (photovoltage) to some extent. On the other hand, irreversible degradation induced by oxygen is attributed to calcium oxide formation. In this work, generation of this oxide takes place only to a small degree, which is responsible for a decrease in FF. These conclusions are supported by capacitance–voltage measurements, which provide values for degree of oxygen doping levels in the films and evidences for CaO generation.

Acknowledgments

We thank financial support from Ministerio de Educacion y Ciencia under Project HOPE CSD2007-00007 (Consolider-Ingenio

2010), Generalitat Valenciana under Project PROMETEO/2009/058 and Conselho Nacional de Desenvolvimento Científico e Tecnológico (CNPq) under Process 201380/2010-2.

Appendix A. Supplementary material

Supplementary data associated with this article can be found in the online version at doi:10.1016/j.solmat.2012.01.012.

References

[1] M.A. Green, K. Emery, Y. Hishikawa, W. Warta, Solar cell efficiency tables (version 35), Progress in Photovoltaics 18 (2010) 144–150.
[2] M. Jørgensen, K. Norrman, F.C. Krebs, Stability/degradation of polymer solar cells, Solar Energy Materials and Solar Cells 92 (2008) 686–714.
[3] K. Norrman, S.A. Gevorgyan, F.C. Krebs, Water-induced degradation of polymer solar cells studied by (H_2O)-O-18 labeling, ACS Applied Materials and Interfaces 1 (2009) 102–112.
[4] M.O. Reese, A.J. Morfa, M.S. White, N. Kopidakis, S.E. Shaheen, G. Rumbles, D.S. Ginley, Pathways for the degradation of organic photovoltaic P3HT:PCBM based devices, Solar Energy Materials and Solar Cells 92 (2008) 746–752.
[5] M. Manceau, A. Rivaton, J.L. Gardette, S. Guillerez, N. Lemaitre, The mechanism of photo- and thermooxidation of poly(3-hexylthiophene) (P3HT) reconsidered, Polymer Degradation and Stability 94 (2009) 898–907.
[6] H.J. Kim, H.H. Lee, J.J. Kim, Real time investigation of the interface between a P3HT:PCBMlayer and an Al electrode during thermal annealing, Macromolecular Rapid Communications 30 (2009) 1269–1273.
[7] C.F. Zhang, Y. Hao, S.W. Tong, Z.H. Lin, Q.A. Feng, E.T. Kang, C.X. Zhu, Effects of cathode confinement on the performance of polymer/fullerene photovoltaic cells in the thermal treatment, IEEE Transactions on Electron Devices 58 (2011) 835–842.
[8] F.C. Krebs, S.A. Gevorgyan, J. Alstrup, A roll-to-roll process to flexible polymer solar cells: model studies, manufacture and operational stability studies, Journal of Materials Chemistry 19 (2009) 5442–5451.
[9] J. Schafferhans, A. Baumann, C. Deibel, V. Dyakonov, Trap distribution and the impact of oxygen-induced traps on the charge transport in poly(3-hexylthiophene), Applied Physics Letters 93 (2008) 093303.
[10] A. Tapponnier, I. Biaggio, P. Gunter, Ultrapure C-60 field-effect transistors and the effects of oxygen exposure, Applied Physics Letters 86 (2005) 112114.
[11] T. Matsushima, M. Yahiro, C. Adachi, Estimation of electron traps in carbon-60 field-effect transistors by a thermally stimulated current technique, Applied Physics Letters 91 (2007) 103505.
[12] M.T. Lloyd, D.C. Olson, P. Lu, E. Fang, D.L. Moore, M.S. White, M.O. Reese, D.S. Ginley, J.W.P. Hsu, Impact of contact evolution on the shelf life of organic solar cells, Journal of Materials Chemistry 19 (2009) 7638–7642.
[13] M.S.A. Abdou, F.P. Orfino, Y. Son, S. Holdcroft, Interaction of oxygen with conjugated polymers: charge transfer complex formation with poly(3-alkylthiophenes), Journal of the American Chemical Society 119 (1997) 4518–4524.
[14] A. Aguirre, S.C.J. Meskers, R.A.J. Janssen, H.-J. Egelhaaf, Formation of metastable charges as a first step in photoinduced degradation in p-conjugated polymer: fullerene blends for photovoltaic applications, Organic Electronics 12 (2011) 1657–1662.
[15] M. Manceau, A. Rivaton, J.L. Gardette, Involvement of singlet oxygen in the solid-state photochemistry of P3HT, Macromolecular Rapid Communications 29 (2008) 1823–1827.
[16] H. Hintz, H.J. Egelhaaf, L. Luer, J. Hauch, H. Peisert, T. Chasse, Photodegradation of P3HT—a systematic study of environmental factors, Chemistry of Materials 23 (2011) 145–154.
[17] A. Seemann, T. Sauermann, C. Lungenschmied, O. Armbruster, S. Bauer, H.J. Egelhaaf, J. Hauch, Reversible and irreversible degradation of organic solar cell performance by oxygen, Solar Energy 85 (2011) 1238–1249.
[18] S.J. Wu, J.H. Li, Q.D. Tai, F. Yan, Investigation of high-performance air-processed poly(3-hexylthiophene)/methanofullerene bulk-heterojunction solar cells, Journal of Physical Chemistry C 114 (2010) 21873–21877.
[19] A. Guerrero, K. Kulbaba, M. Bochmann, Alkyl zinc chlorides as new initiators for the polymerization and copolymerization of isobutene, Macromolecular Chemistry and Physics 209 (2008) 1714–1720.
[20] B.A. Mattis, P.C. Chang, V. Subramanian, Performance recovery and optimization of poly(3-hexylthiophene) transistors by thermal cycling, Synthetic Metals 156 (2006) 1241–1248.
[21] G. Li, V. Shrotriya, J.S. Huang, Y. Yao, T. Moriarty, K. Emery, Y. Yang, High-efficiency solution processable polymer photovoltaic cells by self-organization of polymer blends, Nature Materials 4 (2005) 864–868.
[22] J. Hwang, D.B. Tanner, I. Schwendeman, J.R. Reynolds, Optical properties of nondegenerate ground-state polymers: three dioxythiophene-based conjugated polymers, Physical Review B 67 (2003) 115205.
[23] F. Fabregat-Santiago, G. Garcia-Belmonte, I. Mora-Seró, J. Bisquert, Characterization of nanostructured hybrid and organic solar cells by impedance spectroscopy, Physical Chemistry and Chemical Physics 13 (2011) 9083–9118.
[24] P.P. Boix, A. Guerrero, L.F. Marchesi, G. Garcia-Belmonte, J. Bisquert, Current–voltage characteristics of bulk heterojunction organic solar cells: connection between light and dark curves, Advanced Energy Materials 1 (2011) 1073–1078.
[25] J. Bisquert, G. Garcia-Belmonte, A. Munar, M. Sessolo, A. Soriano, H.J. Bolink, Band unpinning and photovoltaic model for P3HT–PCBM organic bulk heterojunctions under illumination, Chemical Physics Letters 465 (2008) 57–62.
[26] H. Ishii, N. Hayashi, E. Ito, Y. Washizu, K. Sugi, Y. Kimura, M. Niwano, Y. Ouchi, K. Seki, Kelvin probe study of band bending at organic semiconductor/metal interfaces: examination of Fermi level alignment, Physica Status Solidi A: Applied Research 201 (2004) 1075–1094.